A Three-Actuator Cable-Driven Parallel Robot With a Rectangular Workspace

Foroogh Behroozi, Ramin Mersi, Antoine Benoist, Ru Ying Yong, Philippe Cardou, Stéphane Caro

A Three-Actuator Cable-Driven Parallel Robot with a Rectangular Workspace

Foroogh Behroozi
Email: foroogh.behroozi.1@ulaval.ca
Ramin Mersi
Email: ramin.mersi.1@ulaval.ca
Antoine Benoist
Email: antoinebenoist256@gmail.com
Ru Ying Yong
Email: ru-ying.yong@insa-lyon.fr
Philippe Cardou
Email: philippe.cardou@gmc.ulaval.ca

Laboratoire de robotique
Department of Mechanical Engineering
Université Laval
Québec, QC, Canada, G1V 0A6

Stéphane Caro

Nantes Université
École Centrale Nantes
CNRS, LS2N
UMR 6004, 1, rue de la Noe, 44321 Nantes, France
Email: stephane.caro@ls2n.fr

In the realm of cable-driven parallel robots (CDPRs), the conventional notion entails that each cable is directly actuated by a corresponding actuator, implying a direct relationship between the number of cables and actuators. However, this paper introduces a paradigm shift by contending that the number of cables should be contingent upon the desired workspace, while the number of actuators should align with the robot's degrees of freedom (DoF). This novel perspective leads to an unconventional design methodology for CDPRs. Instead of commencing with the number of actuators and cables in mind, we propose an approach that begins with defining the required workspace shape and determines the requisite number of cables. Subsequently, an actuation scheme is established where each actuator can drive multiple cables. This process entails the formulation of a transmission matrix that captures the interplay between actuators and cables, followed by the mechanical implementation of the corresponding cable-pulley routing. To illustrate this approach, we provide an example involving a 2-DoF CDPR aimed at covering a rectangular workspace. Notably, the resulting Wrench-Closure Workspace (WCW) and Wrench-Feasible Workspace (WFW) of the proposed designs exhibit favorable comparisons to existing CDPRs with more actuators.

1 INTRODUCTION

Cable robots are typically categorized into three distinct classes, contingent upon the quantity of cables and actuators: under-constrained, fully-constrained, and over-constrained [1, 2, 3, 4, 5, 6]. While the presence of redundancy in actuation becomes imperative owing to the unilateral behavior of cables, which solely facilitate tension forces [7, 8], the concept of underactuation represents a well-established notion in the realm of robotics [9, 10, 11, 12, 13]. At its core, it signifies having fewer inputs than outputs, and fewer actuators than degrees of freedom. Interestingly, the strategic allocation of a larger number of cables than actuators can yield the dual benefits of expanded workspace and reduced complexity in the design of CDPRs [14, 15].

One of the prevalent architectural choices for planar CDPRs is meant to encompass a rectangular workspace, typically involving four cables and four actuators (see Fig. 1(a)). This configuration imparts an actuation redundancy of two to a CDPR equipped with four cables and a

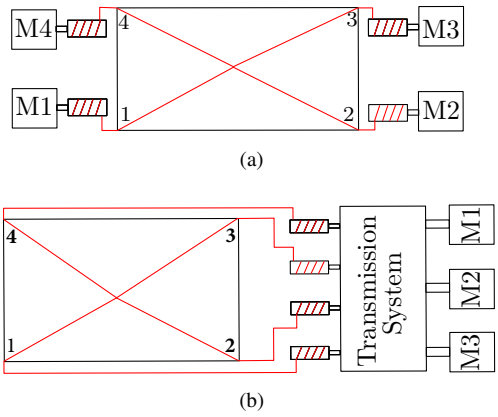

Fig. 1: Planar CDPRs with four cables and a point-mass end-effector: (a) having four actuators; (b) using a transmission system to drive four cables with three actuators

point-mass end-effector. To ensure a wrench-closure state for the end-effector, an n-DoF CDPR generally requires a minimum of $n+1$ actuated cables, given the constraint that cables can exert tension but not compression. In the context of the 2-DoF planar CDPR with a point-mass end-effector under examination, this translates to a minimum requirement of three actuators, resulting in an excess of one actuator. The presence of additional actuator(s) adds to the robot cost and complexity which prompts the exploration of alternatives. Our approach consists in retaining the existing four cables, while seeking a transmission system that permits their operation with just three actuators, as depicted in Fig. 1(b).

Birglen and Gosselin [16] delved into the force transmission attributes of fingers in configurations of underactuation. In [17], the same authors present a thorough investigation into the kinetostatic analysis of underactuated fingers within robotic systems. The study conducted in [18] encompasses a comprehensive exploration of the design and applications of an optimally unstable underactuated gripper. Furthermore, [19] offers an in-depth examination of geometric design considerations pertaining to three-phalanx underactuated fingers, showcasing transmission mechanisms either of linkages or tendons and pulleys. The same authors, in [20], propose a method for analyzing the force capabilities of interconnected differential mechanisms, namely, a pivotal aspect in extending the underactuation principle from fingers to the encompassing hand. Additionally, [21] introduces an underactuated hand featuring five actuators, adept at executing a spectrum of grasping and in-hand repositioning tasks.

Cable-pulley transmission systems offer a distinct amalgamation of advantages, including zero-backlash motion, high stiffness, low stiction, and reduced friction, rendering them highly desirable for applications involving force and torque control [22]. In [23], Kevac and Filipovic presented a comprehensive overview of diverse construction modeling methodologies in cable-suspended parallel robots (CSPRs). They outlined six categories of CSPR systems designed for camera carriers, capable of covering the rectangular workspace using only three actuators instead of the conventional four. While they did not specify the exact percentage of the desired workspace area covered by their proposed concepts, their work introduced an innovative approach to optimizing actuation in cable-suspended parallel robots.

In [24], researchers addressed the challenge of ensuring that the orientation of a CDPR moving platform (MP) remains independent from moments generated by the cable loops. The aim is to achieve this while utilizing no more actuators than the number of degrees of freedom of the CDPR. The solution introduced is a planar Cable-Driven Parallel Crane design, featuring the MP with an embedded mechanism and a specialized transmission module. The MP's connection to the framework involves a triple parallel cable arrangement that constrains orientation and includes a cable loop for actuating the embedded mechanism. The design and fabrication of the transmission system allow it to control over both the double parallelogram's dimensions and the cable loop's circulation. This approach results in a robotic system with three actuators and DoF.

In [25], two novel architectures for planar spring-loaded CDPRs that do not require actuation redundancy are proposed. The authors combine springs with a cable-loop system to eliminate the need for actuator redundancy, allowing for N actuators to control N-DoF motion. The proposed method ensures that the cables and springs are kept in tension within a rectangular workspace, but preloading of the springs is required to cover the entire workspace. The authors suggest that appropriate adjustments to the portion of stiffness and preload can increase the workspace.

The exploration of pulleys and additional cables as a means to reduce the number of actuators in CDPRs has been previously investigated [26, 27, 4]. The idea of employing cable differentials in the design of both spatial and planar CDPRs has been introduced in [26, 27]. The authors primarily focus on comparing outcomes attained by employing a single actuator alongside an increased number of cables and differentials to ascertain the extent of workspace coverage [26]. In [27], the authors resort to differentials to drive multiple cables of a planar CDPR through a single actuator, thereby minimizing the total

number of actuators required. Their findings demonstrate that, for a given number of actuators, the implementation of differentials can result in larger workspaces and enhanced kinetostatic performances. Notably, they covered the triangular shape of the WCW using three actuated cables.

In [4], a configuration for planar CDPRs that utilizes parallelogram links instead of conventional links is presented. The use of parallelogram links ensures that the cables remain in tension during the robot movements, thereby enhancing its dexterity and stiffness. The authors take advantage of cable redundancy to preserve the robot's structure while employing three actuators in the design of planar CDPRs. In this research, a general formulation for parallelogram links is provided to support the suitable design of planar CDPRs. Although the proposed structure is applied to both fully constrained actuated and redundantly actuated configurations, it is unable to cover the entire rectangular workspace.

In our prior work [28], we designed a transmission system that enabled actuators to drive multiple cables through the use of a transmission matrix and corresponding cable-pulley routing. In that paper, we introduced novel cable robot architectures with the minimization number of actuators while simultaneously preserving a rectangular WCW. These architectures diverge from traditional cable robot designs, which conventionally maintain a one-to-one correspondence between cables and actuators. In the proposed architectures, a single cable can be associated with multiple actuators, and vice versa, leading to a reduction in the overall number of required actuators.

In a general scenario, if a CDPR with n degrees of freedom is driven by p actuators and does not depend on external forces like gravity to maintain cable tension, a necessary equilibrium condition is given by $p \geq n+1$. To effectively describe the interplay between actuators and driving cables, we employ the transmission matrix mapping the actuator torques onto the resulting cable tensions. We determine which transmission matrices are equivalent from the standpoint of wrench-closure of the end-effector and we propose a unique representation for these linear subspaces of equivalent matrices. Alongside this, we present a new expression for the WCW and an organized synthesis method for determining optimal values for the previously proposed transmission system in [28], with the objective of expanding the robot's workspace.

The organization of this paper is as follows. The foundational mathematical groundwork for the kinetostatic analysis of n-degree of freedom (n-DoF), m-cable, p-actuator CDPRs is presented in Section 2. Section 3 delves into the formulation of the transmission matrix for the synthesis of the optimization problem, which is formulated to determine the optimal values that yield the maximum area for the WCW. Section 4 then presents the solution to this synthesis problem, its embodiment, WCW, wrench-feasible workspace (WFW), and experimental validation; finally, the conclusions are presented in Section 5.

2 KINETOSTATIC ANALYSIS

In this section, we present the kinetostatic analysis of the proposed n-DoF m-cable p-actuator planar CDPR. The equations of equilibrium of the end-effector can be written as Eq. (1), as reported in [29].

$$\mathbf{W}\mathbf{t} + \mathbf{w}_e = \mathbf{0}_n \quad , \quad \mathbf{t} > \mathbf{0}_m, \tag{1}$$

where $\mathbf{W} \in \mathbb{R}^{n\times m}$ is the wrench matrix of the cable robot when its end-effector is located at pose $\mathbf{p}$, $\mathbf{w}_e$ is the external wrench and $\mathbf{t}$ is the array of cable tensions. The WCW is the set of poses of the end effector where any wrench can be generated at the end effector by tightening the cables [30]. Roberts et al. [31] showed that a given pose lies inside the WCW (i.e., is wrench closure) if and only if one can find a vector $\mathbf{t}_\perp > \mathbf{0}_m$ in the nullspace of $\mathbf{W}$, where $>$ indicates a componentwise strict inequality.

In our case, however, not all the tensions found in the nullspace of $\mathbf{W}$ can be generated from $p < m$ actuators. Let us define matrix $\mathbf{T} \in \mathbb{R}^{m\times p}$, which represents the linear transmission between actuators and winches. The matrix $\mathbf{T}$ maps the actuator torques $\boldsymbol{\tau} \in \mathbb{R}^p$ onto the cable tensions $\mathbf{t} \in \mathbb{R}^m$, namely,

$$\mathbf{t} = \mathbf{T}\boldsymbol{\tau}. \tag{2}$$

To determine whether there exists a solution $(\mathbf{T}, \boldsymbol{\tau})$ to Eqs. (1) and (2) for any external wrench $\mathbf{w}_e \in \mathbb{R}^n$, we must identify a positive vector $\mathbf{t}$ that lies simultaneously within the nullspace of the wrench matrix $\mathbf{W}(\mathbf{p})$ and in the range[1] of matrix $\mathbf{T}$. To accomplish this, we recast Eqs. (1) and (2) into matrix form, which yields:

$$\begin{bmatrix} \mathbf{W} & \mathbf{0}_{n\times p} \\ \mathbf{1}_{m\times m} & -\mathbf{T} \end{bmatrix} \begin{bmatrix} \mathbf{t} \\ \boldsymbol{\tau} \end{bmatrix} = \begin{bmatrix} \mathbf{0}_n \\ \mathbf{0}_m \end{bmatrix}, \tag{3}$$

[1] The range (a.k.a. the column space or image) of a matrix is the span of its column vectors.

where $\mathbf{1}_{m\times m}$ is the $m \times m$ identity matrix and $\mathbf{0}_{n\times p}$ is the $n \times p$ zero matrix. The solution to Eq. (3) amounts to computing the nullspace of the $(m + n) \times (m + p)$ matrix and verifying whether $\mathbf{t} > \mathbf{0}_m$. As $p = n + 1$, the number of columns is one more than the number of rows and this matrix has a rank of $m + n$ unless one of $\mathbf{W}$ and $\mathbf{T}$ is rank-deficient. To compute this nullspace symbolically, let us modify it by adding two vectors of dummy variables: $\mathbf{z}_1 \in \mathbb{R}^m$ and $\mathbf{z}_2 \in \mathbb{R}^p$, as the first row of the matrix of Eq. (3). This yields the square matrix

$$\mathbf{A} = \begin{bmatrix} \mathbf{z}_1^T & \mathbf{z}_2^T \\ \mathbf{W}_{n\times m} & \mathbf{0}_{n\times p} \\ \mathbf{1}_{m\times m} & -\mathbf{T}_{m\times p} \end{bmatrix} \tag{4}$$

Lemma 1. Let $\mathbf{z}$ be any vector in $\mathbb{R}^{m+p}$, let $\mathbf{W'} \in \mathbb{R}^{(m+n)\times(m+n+1)}$ be of full rank, and let us define

$$\begin{aligned} \mathbf{A} &\equiv \begin{bmatrix} \mathbf{z}^T \\ \mathbf{W'} \end{bmatrix} \in \mathbb{R}^{(m+n+1)\times(m+n+1)} \text{ and} \\ \mathbf{x}_\perp &\equiv \frac{\partial \det(\mathbf{A})}{\partial \mathbf{z}}. \end{aligned} \tag{5}$$

Then $\mathbf{x}_\perp$ is different from $0_{(m+n+1)}$ and lies in the nullspace of $\mathbf{W}'$, i.e., $\mathbf{W}'\mathbf{x}_\perp = \mathbf{0}_{(m+n)}$.

Proof. If we let $\det(\mathbf{A})$ be the determinant of $\mathbf{A}$, then, by definition, we have

$$\mathbf{A}\text{adj}(\mathbf{A}) = \det(\mathbf{A})\mathbf{1}_{(m+n+1)\times(m+n+1)}. \tag{6}$$

where $\text{adj}(\mathbf{A})$ is the adjoint of $\mathbf{A}$. Let us partition this matrix as $\text{adj}(\mathbf{A}) = [\boldsymbol{\alpha}\ \boldsymbol{\Gamma}]$, where $\boldsymbol{\alpha} \in \mathbb{R}^{m+n+1}$ and $\boldsymbol{\Gamma} \in \mathbb{R}^{(m+n+1)\times(m+n)}$. This allows us to rewrite eq. (6) as

$$\begin{aligned} \begin{bmatrix} \mathbf{z}^T \\ \mathbf{W'} \end{bmatrix} [\boldsymbol{\alpha}\ \boldsymbol{\Gamma}] &= \begin{bmatrix} \mathbf{z}^T\boldsymbol{\alpha} & \mathbf{z}^T\boldsymbol{\Gamma} \\ \mathbf{W}'\boldsymbol{\alpha} & \mathbf{W}'\boldsymbol{\Gamma} \end{bmatrix} \\ &= \begin{bmatrix} \det(\mathbf{A}) & \mathbf{0}_{m+n}^T \\ \mathbf{0}_{m+n} & \det(\mathbf{A})\mathbf{1}_{(m+n)\times(m+n)} \end{bmatrix}. \end{aligned} \tag{7}$$

Focusing on the upper-left blocks of this matrix equality, we have the equation $\mathbf{z}^T\boldsymbol{\alpha} = \det(\mathbf{A})$. Because $\mathbf{z}$ appears in exactly one row of $\mathbf{A}$, the properties of determinants allow us to conclude that $\det(\mathbf{A})$ is linear in $\mathbf{z}$. If $\det(\mathbf{A})$ is linear in $\mathbf{z}$ and equal to $\mathbf{z}^T\boldsymbol{\alpha}$, then this implies that $\boldsymbol{\alpha}$ is independent from $\mathbf{z}$. As a result, the differentiation of both sides of $\mathbf{z}^T\boldsymbol{\alpha} = \det(\mathbf{A})$ with respect to $\mathbf{z}$ yields simply

$$\frac{\partial \mathbf{z}^T\boldsymbol{\alpha}}{\partial \mathbf{z}} = \boldsymbol{\alpha} = \frac{\partial \det(\mathbf{A})}{\partial \mathbf{z}} = \mathbf{x}_\perp. \tag{8}$$

Moreover, because $\mathbf{W}'$ is of full rank by assumption, we have $\det(\mathbf{A}) = 0$. This determinant being linear in $\mathbf{z}$, we conclude that its gradient cannot be null, i.e., $\mathbf{x}_\perp = 0_{(m+n+1)}$. On the other hand, the lower-left block of the matrix equality (7) yields

$$\mathbf{W}'\boldsymbol{\alpha} = \mathbf{0}_{m+n}, \tag{9}$$

and therefore $\boldsymbol{\alpha}$ is in the nullspace of $\mathbf{W}'$.

We complete the proof by comparing Eqs. (8) and (9) concluding that

$$\mathbf{x}_\perp = \boldsymbol{\alpha} = \frac{\partial \det(\mathbf{A})}{\partial \mathbf{z}}. \tag{10}$$

□

Using **Lemma 1** to calculate the cable tensions, we can take the partial derivative of the determinant of Eq. (4). As stated in **Lemma 1**, $\mathbf{W}'$ should be of full rank. This condition is satisfied when both $\mathbf{W}_{n\times m}$ and $\mathbf{T}_{m\times p}$ are of full rank. By knowing that $\mathbf{t}_\perp$ is the first column of adj($\mathbf{A}$), the WCW of the proposed CDPR is the set of poses where:

$$\mathbf{t}_\perp = \frac{\partial}{\partial \mathbf{z}_1}\det(\mathbf{A}) > \mathbf{0}_m, \tag{11}$$

Since $\mathbf{t}_\perp$ can be computed in closed form, leaving the pose parameters as variables and equating to zero the entries of $\mathbf{t}_\perp$ yields the potential boundaries of the WCW. In this research the boundary equations were computed in Maple with the code `Gradient(Determinant(A),z1);` but it could be done with any other symbolic computation language. To our best knowledge, this method of tracing the WCW for CDPRs where $\mathbf{T} \neq \mathbf{I}_{m\times m}$ has not been reported before.

The exploration of the impact of various $\mathbf{T}$ matrices

on the WCW area can shed light on the importance of this critical component in the successful implementation of 2-DoF CDPRs with three actuators. As an example, the WCW resulting from two $\mathbf{T}$ matrices are illustrated in Fig. 2. Due to the significance of the $\mathbf{T}$ matrix in determining the WCW area, the next section of this paper focuses on a methodology to optimize the transmission matrix to achieve a rectangular-shaped workspace.

$$\mathbf{T} = \begin{bmatrix} 1 & 1 & 0 \\ 0 & -1 & 1 \\ 1 & -1 & 0 \\ 1 & 0 & -1 \end{bmatrix}$$

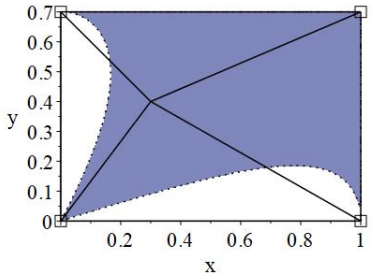

(a)

$$\mathbf{T} = \begin{bmatrix} 1 & 1 & 0 \\ 1 & 1 & 1 \\ 1 & -1 & 0 \\ 1 & 0 & -1 \end{bmatrix}$$

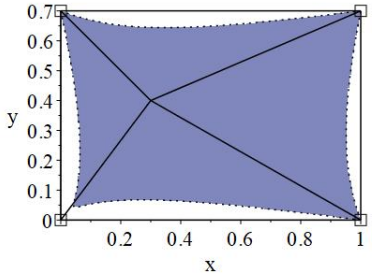

(b)

Fig. 2: Influence of two different transmission matrices on ((a) and (b)) the WCW of a 2-DoF CDPR with three actuators

3 FORMULATION OF THE SYNTHESIS OF THE TRANSMISSION MATRIX

For the 2-DoF three-actuator planar CDPR of Fig. 1(b), we have $\mathbf{T} \in \mathbb{R}^{4\times 3}$. In order to find the optimum value of this matrix, our strategy consists in testing wrench-closure at a number of control points in the workspace. We then maximize the number of such points where wrench-closure is achieved. From Eq. (11), the wrench-closure condition at position $\mathbf{p}_k$ may be determined by solving the problem

$$\begin{array}{lll} \text{maximize} & s_k & \\ \text{subject to} & \dfrac{\partial}{\partial \mathbf{z}_1}\det(\mathbf{A}_k) \geq s_k \mathbf{1}_4, & (12) \\ \text{over} & \mathbf{T},\ s_k, \qquad k = 1, ..., q & \end{array}$$

where $\mathbf{A}_k$ is matrix $\mathbf{A}$ evaluated at $\mathbf{p}_k$. When the solution yields $s_k = 0$, this implies that there is no vector $\frac{\partial}{\partial \mathbf{z}_1}\det(\mathbf{A}_k)$ that is strictly positive. When $s_k \to \infty$, the problem is unbounded and we have wrench-closure at $\mathbf{p}_k$ for the corresponding matrix $\mathbf{T}$. To prevent the problem from being unbounded, we add the constraints $s_k \leq 1, k = 1, ..., q$ which limits s_k within finite values. Upon combining several poses $\mathbf{p}_k$, $k = 1, ..., q$, we obtain the synthesis problem

$$\begin{array}{lll} \text{maximize} & \displaystyle\sum_{k=1}^{q} s_k & \\ \text{subject to} & \dfrac{\partial}{\partial \mathbf{z}_1}\det(\mathbf{A}_k) \geq s_k \mathbf{1}_4, & (13) \\ & s_k \leq 1, \quad k = 1, ..., q & \\ \text{over} & \mathbf{T},\ s_k, \qquad k = 1, ..., q & \end{array}$$

where q is the number of points at which the WCW area is evaluated. The constraints defined in Eq. (13) are of the third-degree in the entries of $\mathbf{T}$, making the optimization problem challenging to solve directly. It can be simplified, however, by exploiting a property of column spaces and echelon forms, by which the range of a matrix and its echelon form are the same. Indeed, going back to the original wrench-closure conditions of Eqs. (1) and (2), we notice that several matrices $\mathbf{T}$ can lead to the same WCW. More specifically, since $\boldsymbol{\tau} \in \mathbb{R}^p$, any two matrices $\mathbf{T}$ that have the same range generate the same subspace in the space of tensions $\mathbb{R}^m$. Therefore, we would like to limit the synthesis problem of Eq. (13) to a unique $\mathbf{T}$ for each possible range in $\mathbb{R}^{m\times p}$. The reduced echelon form of the transpose of $\mathbf{T}$ provides this unique representation of the range (see [32], page 48). Indeed, the reduced echelon forms in $\mathbb{R}^{4\times 3}$ cover all the possible ranges of $\mathbb{R}^4$ and yet no two such matrices can have the same range.

$$\mathbf{T}_e = \begin{bmatrix} 1 & 0 & 0 \\ 0 & 1 & 0 \\ 0 & 0 & 1 \\ v_1 & v_2 & v_3 \end{bmatrix} \tag{14}$$

where v_i will serve as the new variables in the optimization problem. As a result, the updated matrix will be:

$$\mathbf{B} = \begin{bmatrix} \mathbf{z}_1^T & \mathbf{z}_2^T \\ \mathbf{W}_{n\times m} & \mathbf{0}_{n\times p} \\ \mathbf{1}_{m\times m} & -\mathbf{T}_e \end{bmatrix} \tag{15}$$

By replacing the $\mathbf{A}$ matrix with $\mathbf{B}$ into Eq. (11) and computing the partial derivatives, we obtain expressions that are linear in v_1, v_2 and v_3. These linear constraints can be written in the form

$$b_{j0} + b_{j1}v_1 + b_{j2}v_2 + b_{j3}v_3 \geq 0, \tag{16}$$

where $b_{ji},\ j = 1, ..., (m+p),\ i = 0, ..., 3$ represent constant coefficients. The presence of the constant value b_{j0} on the left side of the inequality constraint prevents this linear form from being homogeneous. We would like to have homogeneity because it would make the numerical solution robust, less susceptible to changing tolerances and stopping criteria. To this end, we introduce the substitutions $v_1 = V_1/V_0$, $v_2 = V_2/V_0$, and $v_3 = V_3/V_0$. This leads to the following representation:

$$\begin{aligned} \mathbf{1}'_{m\times m} &= \begin{bmatrix} \mathbf{1}_{(m-1)\times(m-1)} & \mathbf{0}_{m-1} \\ \mathbf{0}^T_{(m-1)} & V_0 \end{bmatrix} \text{ and} \\ \mathbf{T}'_e &= \begin{bmatrix} 1 & 0 & 0 \\ 0 & 1 & 0 \\ 0 & 0 & 1 \\ V_1 & V_2 & V_3 \end{bmatrix}. \end{aligned} \tag{17}$$

The final matrix is represented as $\mathbf{B}'$ as follows:

$$\mathbf{B}' = \begin{bmatrix} \mathbf{z}_1^T & \mathbf{z}_2^T \\ \mathbf{W}_{n\times m} & \mathbf{0}_{n\times p} \\ \mathbf{1}'_{m\times m} & -\mathbf{T}'_e \end{bmatrix}. \tag{18}$$

Upon entering these changes in the optimization problem as defined in Eq. (13), we obtain the following new form:

$$\begin{aligned} \text{maximize} \quad & \sum_{k=1}^{q} s_k \\ \text{subject to} \quad & \frac{\partial}{\partial \mathbf{z}_1}\det(\mathbf{B}'_k) \geq s_k \mathbf{1}_4, \\ & s_k \leq 1, \quad k = 1, ..., q \\ \text{over} \quad & V_i,\ i = 0, ..., 3, \quad s_k. \end{aligned} \tag{19}$$

As evidenced in Eq. (19), the optimization problem involves five constraints for each central point where wrench-closure is tested. This constraint count will increase with the addition of more points. By exploiting properties of determinants, the constraints in Eq. (19) can be formulated as follows:

$$b_{j0}V_0 + b_{j1}V_1 + b_{j2}V_2 + b_{j3}V_3 \geq s_k. \tag{20}$$

As a result, Eq. (19) is a linear problem, a class of optimization problems that is well known. There exist methods that are very efficient to solve this type of problem, even for high numbers of constraints. Because they are convex, one can always find the global maximum if it exists.

4 SOLUTION OF THE SYNTHESIS OF THE TRANSMISSION MATRIX

Consider the scenario of the 2-DoF CDPR depicted in Fig. 1(b). In this configuration, the objective is to determine the transmission matrix that allows its particle end-effector to cover a workspace that closely approximates the rectangular region formed by the fixed attachment points of its four cables.

4.1 Determination of the transmission matrix T of the 2-DoF CDPR

As previously mentioned, the number of constraints grows in tandem with the increasing number of control points. In addressing problem (19), an in-depth analysis involving 40 points was conducted, resulting in a total of 200 constraints for the problem. Each position was meticulously chosen with a spacing of 0.0001 inside the specified boundaries of the desired rectangular workspace the

dimension of which are 0.7 m $\times$ 1 m (Fig. 3). The resolution of the problem was executed through the application of the `LPSolve` function within Maple, yielding the optimal values: $V_0 = 1.627 \times 10^{-10}, V_1 = 1.631 \times 10^{-10}, V_2 = -1.633 \times 10^{-10}, V_3 = 1.641 \times 10^{-10}$. Subsequently, the $\mathbf{T}_e$ matrix is obtained from Eq. (14). Because the solution to the linear program also yields $s_k = 1$, $k = 1$, ..., 40, we conclude that the WCW of this robot encompasses all 40 control points. However, it is necessary to verify a posteriori whether the full rectangle is included in the WCW.

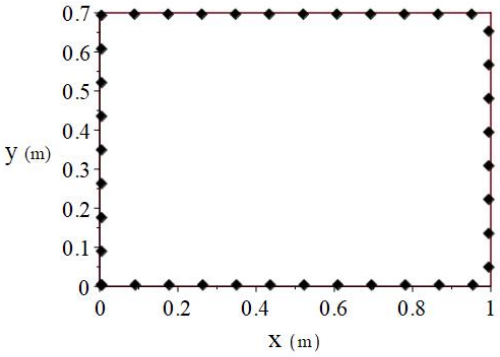

Fig. 3: Control points which are defined for the constraints in Eq. (19)

$$\mathbf{T}_e = \begin{bmatrix} 1 & 0 & 0 \\ 0 & 1 & 0 \\ 0 & 0 & 1 \\ 1.0022 & -1.0039 & 1.0085 \end{bmatrix}. \tag{21}$$

The last row of the $\mathbf{T}_e$ matrix in Eq. (21), $[1.0022 \; -1.0039 \; 1.0085]$ is very close to $[1 \; -1 \; 1]$, so

$$\mathbf{T}_e = \begin{bmatrix} 1 & 0 & 0 \\ 0 & 1 & 0 \\ 0 & 0 & 1 \\ 1 & -1 & 1 \end{bmatrix}. \tag{22}$$

This convergence arises because the last row of the $\mathbf{T}_e$ matrix delineates the directions of the actuator forces. This validates our intuitive understanding of the pivotal role played by the last row of $\mathbf{T}_e$.

To facilitate the mechanical design of the robot, we should not limit ourselves to $\mathbf{T}_e$, but instead consider any 4×3 matrix whose range corresponds to that of $\mathbf{T}_e$. A workable $\mathbf{T}$ matrix was identified by linearly combining the columns of the $\mathbf{T}_e$ while looking for symmetry in the system. It has a range identical to that of $\mathbf{T}_e$, thereby producing an identical wrench-closure workspace:

$$\mathbf{T} = \begin{bmatrix} 1 & 1 & 0 \\ 1 & 0 & 1 \\ 1 & -1 & 0 \\ 1 & 0 & -1 \end{bmatrix}. \tag{23}$$

The WCW of each matrix remains consistent with that of the $\mathbf{T}_e$ matrix.

The value of the element $T_{i,j}$ of $\mathbf{T}$ is $T_{i,j} = 1$ when the i^{th} cable is directly connected to the j^{th} actuator, and $T_{i,j} = -1$ when the i^{th} cable is connected to the j^{th} actuator in reverse. $T_{i,j} = 0$ when the i^{th} cable is not connected to the j^{th} actuator. The second actuator needs to connect to cables one and three, while the third actuator connects to cables two and four. When the second actuator winds the first cable, it simultaneously unwinds the third cable at the same rate. Similarly, the relationship between cable numbers two and four holds for the third actuator.

Having defined $\mathbf{T}$, our focus now shifts towards computing its associated WCW. This computation follows the method elaborated in Section 2, which leads to the WCW depicted in Fig. 4(a). As illustrated, the WCW of this robot effectively encompasses the entire rectangle defined by the fixed cable attachment points. In Fig. 4(b), we present the WCW of a comparable Cable-Driven Parallel Robot (CDPR) proposed in [4], which covered most but not all of the rectangular workspace. Utilizing Maple 2018, we derived symbolic expressions for the workspace boundaries using the four inequalities $\mathbf{t}_\perp = \frac{\partial}{\partial \mathbf{z}_1} \det(\mathbf{A}) > \mathbf{0}_4$. The boundaries of the workspace in the Cartesian plane, given by $\mathbf{t}_\perp(x, y) = \mathbf{0}_4$, are nonlinear and non-algebraic in terms of x and y.

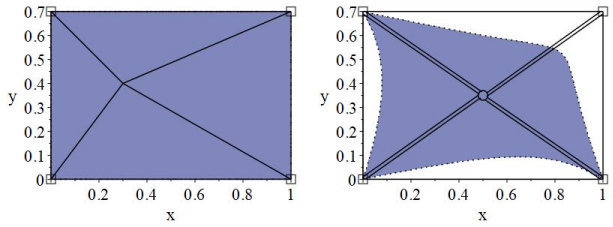

(a) (b)

Fig. 4: Comparison of two 2-DoF, 3-actuator CDPRs: (a) WCW corresponding to the optimum transmission matrix in Eq. (22), (b) WCW of the planar CDPR proposed in [4].

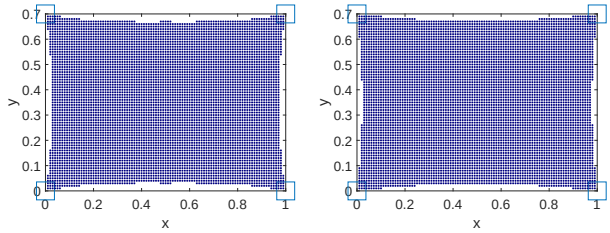

(a) (b)

Fig. 5: WFW of the CDPR considering $-0.5N \leq f_x \leq 0.5N$ and $-0.5N \leq f_y \leq 0.5N$ external forces: (a) proposed CDPR; (b) classic CDPR.

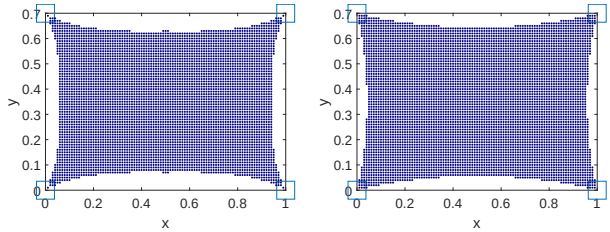

(a) (b)

Fig. 6: WFW of the CDPR considering $-2.5N \leq f_x \leq 2.5N$ and $-2.5N \leq f_y \leq 2.5N$ external forces: (a) proposed CDPR; (b) classic CDPR.

4.2 Determination of the Wrench-Feasible-Workspace of a 2-DoF CDPR

The Wrench-Feasible Workspace (WFW) is defined as the collection of platform poses where all the wrenches within a specified set can be balanced using tension forces in the cables, while ensuring that the cable tensions satisfy the prescribed limits [30, 33]. The determination of the WFW for the CDPR is formulated as a constraint satisfaction problem, as defined in Eq. (24).

$$\begin{aligned} \text{satisfy} \quad & \mathbf{W}\mathbf{t} = \mathbf{w}_e, \\ & \mathbf{t} - \mathbf{T}\boldsymbol{\tau} = \mathbf{0}_4, \\ & \mathbf{1}_4 \leq \mathbf{t} \leq 20\mathbf{1}_4, \\ \text{over} \quad & \mathbf{t}, \boldsymbol{\tau}, \end{aligned} \tag{24}$$

where $\mathbf{W}$ is constant for a given pose $\mathbf{p}$ and $\mathbf{T}$ is the constant optimum value given in Eq. (22).

The first constraint in Eq. (24) ensures that the external wrench can be balanced at the platform pose $\mathbf{p}$. The second constraint represents the relationship between cable tensions and the actuator torques. The effect of the third constraint is to maximize the minimum cable tensions. The fourth constraint ensures that cable tensions are bounded between 1 N and 20 N, reflecting the characteristics of the cables and actuators employed in the CDPR prototype.

We investigated the WFW with drum radius values of $R_1 = R_2 = R_3 = 25$ mm, while imposing tension limits of 1 N and 20 N (Figs. 5(a), 6(a), 7(a)). Our observations reveal that the WFW exhibits an approximately rectangular shape, but its scale diminishes as the external force range increases. In contrast, the WFW of the conventional variant of the 2-DoF planar CDPR with four actuators is depicted in Figs. 5(b), 6(b), 7(b). The comparison between the WFWs of the proposed and classic CDPRs shows that going from four to three motors contracts the WFW, but not dramatically. The dynamic workspace can be computed as a special case of the WFW where the external wrenches are the inertial forces of the moving platform. Accordingly, one can expect a similar comparison between the dynamic workspaces of the proposed and classic CDPRs. We conjecture that the dynamic workspace of the proposed CDPR would be somewhat smaller than that of the classic CDPR, for the same dynamic characteristics.

Having established the ability of the proposed CDPR architecture to achieve wrench closure across the entire rectangular region defined by its fixed attachment points using three actuators, let us shift our focus to devising a practical implementation of this theoretical design.

4.3 Embodiment of the Transmission System in the 2-DoF Planar CDPR

To implement the proposed transmission matrix, we opted for a cable-pulley transmission system to distribute

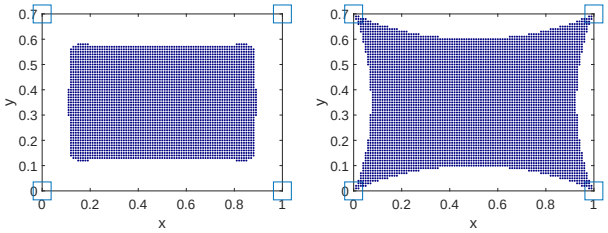

(a) (b)

Fig. 7: WFW of the CDPR considering $-5N \leq f_x \leq 5N$ and $-5N \leq f_y \leq 5N$ external forces: (a) proposed CDPR; (b) classic CDPR.

the power of the three actuators among the four cables. The schematic of the cable routing corresponding to the transmission matrix of Eq. (23) is shown in Fig. 8(a).

In order to reach this cable routing, we proceeded by first observing the connections between each actuator and cable dicated by the transmission matrix. We then attempted to reach this connectivity through trials and errors, by drawing cable routings that were likely to replicate this mapping. For instance, consider the first actuator, which has a relationship with all cables as represented in the $\mathbf{T}$ matrix by the first column $[1\ 1\ 1\ 1]^T$. To achieve the goal of controlling all cables with a single actuator, we incorporated two suspended pulleys. Given that the second column of the optimum $\mathbf{T}$ in Eq. (23) is $[1\ 0\ -1\ 0]^T$, the second actuator should control the first and third cables, but in opposite directions. The second actuator should wind the first cable while simultaneously unwinding the third cable. Similarly, the third actuator should control the second and fourth cables, in symmetry with the second actuator's operation.

To implement the mechanical design, we selected specific dimensions and components. The workspace dimensions are set at $1\,\text{m} \times 0.7\,\text{m}$, and the radii of all drums are chosen to be $25\,\text{mm}$. For the actuators, we employed Pittman DC motors, Series 9236, which operate at $30.3\,\text{V}$ and have a speed in nominal torque of $749\,\text{rpm}$ with a nominal torque of $0.395\,\text{Nm}$. As illustrated in Fig. 8(a), our approach involves two mobile three-level pulleys, serving as direct controllers for the cables within the workspace. In this configuration, the first actuator facilitates the operation of all moving pulleys, whereas the second and third actuators drive two cable loops concurrently.

To validate the correspondance between the cable routings depicted in Fig. 8(a) and the transmission matrices outlined in Eq. (23), a static analysis of the schematic depicted in Fig. 8(a) was conducted. This analysis led

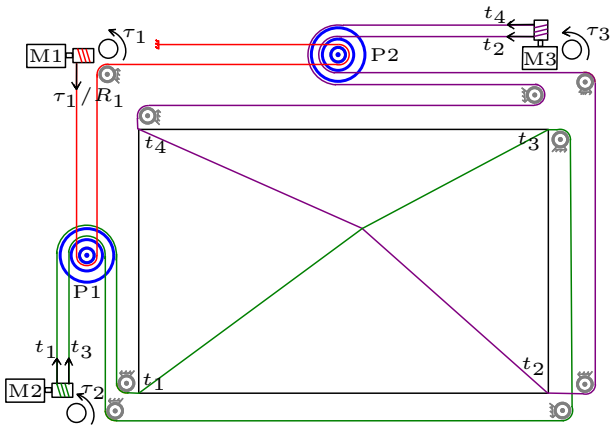

(a)

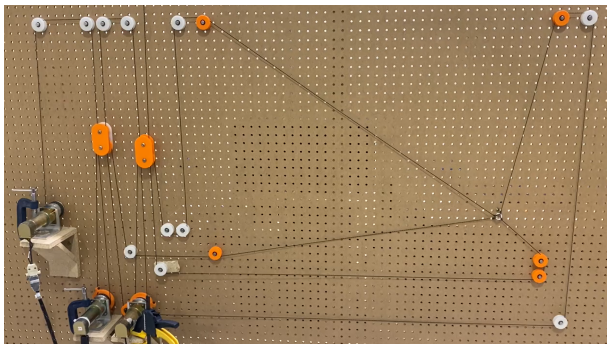

(b)

Fig. 8: The planar CDPR with four cables and a point-mass end-effector driven by three actuators: (a) CDPR proposed schematic; (b) CDPR prototype

to the derivation of the relationship presented in Eq. (30) between actuator torques and cable tensions.

The summation of moments acting on the drum of actuator two results in the expression:

$$\sum M_{M_2} = R_2 t_3 + \tau_2 - R_2 t_1 = 0, \tag{25}$$

where R_2 denotes the radius of drum two. Additionally, the summation of forces exerted on the first pulley is given by:

$$\sum f_{P_1} = t_3 + t_1 - \frac{\tau_1}{R_1} = 0, \tag{26}$$

where R_1 represents the radius of drum one. By subtract-

ing $1/R_2$ of Eq. (25) from Eq. (26), we obtain:

$$\begin{aligned} t_3 + t_1 - \frac{\tau_1}{R_1} - t_3 + t_1 - \frac{\tau_2}{R_2} = 0, \\ 2t_1 = \frac{\tau_1}{R_1} + \frac{\tau_2}{R_2}, \\ t_1 = \left[\tfrac{1}{2R_1}\ \tfrac{1}{2R_2}\ 0\right]\boldsymbol{\tau}. \end{aligned} \tag{27}$$

Then, by adding $1/R_2$ from Eq. (26) to Eq. (25), we get:

$$\begin{aligned} t_3 + t_1 - \frac{\tau_1}{R_1} + t_3 - t_1 + \frac{\tau_2}{R_2} = 0, \\ 2t_3 = \frac{\tau_1}{R_1} - \frac{\tau_2}{R_2}, \\ t_3 = \left[\tfrac{1}{2R_1}\ -\tfrac{1}{2R_2}\ 0\right]\boldsymbol{\tau}. \end{aligned} \tag{28}$$

Following the same method, the sum of moments on the drum of the third actuator yields:

$$\sum M_{M_3} = R_3 t_4 + \tau_3 - R_3 t_2 = 0, \tag{29}$$

where R_3 is the third drum radius.

By summing the forces acting on the second moving pulleys and solving the resulting equation and Eq. (29) for t_2 and t_4, we obtain $t_2 = \left[\frac{1}{2R_1}\ 0\ \frac{1}{2R_3}\right]\boldsymbol{\tau}$ and $t_4 = \left[\frac{1}{2R_1}\ 0\ \frac{-1}{2R_3}\right]\boldsymbol{\tau}$. Upon assembling the latter equations along with Eqs. (27) and (28), we obtain the desired relationship:

$$\mathbf{T}' = \begin{bmatrix} \frac{1}{2R_1} & \frac{1}{2R_2} & 0 \\ \frac{1}{2R_1} & 0 & \frac{1}{2R_3} \\ \frac{1}{2R_1} & -\frac{1}{2R_2} & 0 \\ \frac{1}{2R_1} & 0 & -\frac{1}{2R_3} \end{bmatrix}. \tag{30}$$

In this matrix, $\mathbf{R}_i$ represents the radius of the drum associated with the i^{th} actuator. When all the drums share the same radius, i.e., $R_1 = R_2 = R_3 = R$, it follows that $\mathbf{T} = 2R\mathbf{T}'$.

In order to validate the practical feasibility and performance of the proposed CDPR design, a prototype, shown in Fig. 8(b), was built. This prototype embodies the innovative architecture that reduces the number of actuators while preserving a rectangular WCW. To witness the capabilities of our prototype in action, we invite the reader to view a demonstration video on YouTube [https://youtu.be/qmGK_-rO6Ds]. This video showcases the ability of the robot to cover the wrench-feasible workspace.

The observed limitation preventing the robot from reaching the corners of the workspace is attributed to the limited actuator torques. Nevertheless, the robot maintains a rectangular WFW, even though the corners of the rectangle remain unattainable due to these limited input torques (see Figs. 5(a), 6(a), 7(a)). This demonstration provides an understanding of the robot's capabilities and limitations, accounting for real-world influences.

5 CONCLUSIONS

In this research, we introduced a novel approach to the design of planar CDPRs with fewer actuators than cables, achieved through suitable transmission systems. Notably, our approach leads to a 2-DoF CDPR that covers a rectangular WCW with just one less actuator compared to the conventional four-actuator version. While previous researchers have also explored CDPRs with fewer actuators than cables [25, 27, 4], this work differentiates itself through the chosen design methodology. Instead of starting with the selection or enumeration of mechanical components for the transmission system, we first focus on finding the optimum transmission matrix mapping actuator torques onto cable tensions. Once the transmission matrix is established, its implementation is realized using machine components such as cables and pulleys, but alternative components like gears and belts could also have been employed.

Developing this synthesis method also required making some more focused contributions along the way. Among those, let us point out the compact mathematical expression of the WCW boundaries presented in Eq. (11). Because it resorts to mathematical functions that are widely available in symbolic scientific software, it allows to trace the WCW with very few lines of code. We should also mention the unique representation of CDPR transmission sytems through the echelon form of their transmission matrices. This narrows significantly the search space of the associated synthesis problem. Finally, we consider the formulation of this transmission synthesis problem as a standard linear problem. This is an important contribution, since it allows to tackle problems with large numbers of control points and because it guarantees that any feasible transmission matrix found is globally optimum for the chosen control points.

The research presents such a globally optimum trans-

mission matrix for the 2-DoF CDPR, along with a possible mechanical implementation. Furthermore, the analysis is extended to determine the WFW of the 2-DoF CDPR under three different external force scenarios. The CDPR exhibits reasonably good behavior when compared to the WFW of an analogous four-actuator CDPR.

As a next step, the optimization approach for the WCW and WFW of CDPRs will be extended to higher degrees of freedom and spatial CDPR configurations. This is a challenging task, as the optimization problem may become non-linear and non-convex in these cases. It will therefore require a reliable algorithm to solve the optimization problem.

Other avenues of research may also be explored, such as the replacement of wrench-closure conditions with wrench-feasibility conditions in the proposed synthesis method. This would significantly increase the complexity of the ensuing optimization problem, however, as it would become non-convex and larger.

REFERENCES

[1] Bruckmann, T., and Pott, A., 2012, *Cable-driven parallel robots*, Vol. 12 Springer.

[2] Bosscher, P., Riechel, A. T., and Ebert-Uphoff, I., 2006, "Wrench-feasible workspace generation for cable-driven robots," *IEEE Transactions on Robotics,* **22**(5), pp. 890–902.

[3] Yang, G., Pham, C. B., and Yeo, S. H., 2006, "Workspace performance optimization of fully restrained cable-driven parallel manipulators," In 2006 IEEE/RSJ International Conference on Intelligent Robots and Systems, pp. 85–90.

[4] Khodadadi, N., Hosseini, M. I., Khalilpour, S., Taghirad, H., and Cardou, P., 2021, "Kinematic analysis of planar cable-driven robots with parallelogram links," *2021 CCToMM Mechanisms, Machines, and Mechatronics (M3) Symposium*.

[5] Mersi, R., Vali, S., haghighi, M. S., Abbasnejad, G., and Masouleh, M. T., 2018, "Design and control of a suspended cable-driven parallel robot with four cables," In 2018 6th RSI International Conference on Robotics and Mechatronics (IcRoM), pp. 470–475.

[6] Mersi, R., Archambault, L., Therriault-Proulx, F., and Cardou, P., 2023, "A 5-dof cable driven parallel robot for the calibration of radiotherapy machines,".

[7] Carricato, M., and Merlet, J.-P., 2013, "Stability analysis of underconstrained cable-driven parallel robots," *IEEE Transactions on Robotics,* **29**(1), pp. 288–296.

[8] Song, D., Zhang, L., and Xue, F., 2018, "Configuration optimization and a tension distribution algorithm for cable-driven parallel robots," *IEEE Access,* **6**, pp. 33928–33940.

[9] Bergerman, M., and Xu, Y., 1996, "Robust Joint and Cartesian Control of Underactuated Manipulators," *Journal of Dynamic Systems, Measurement, and Control,* **118**(3), 09, pp. 557–565.

[10] Moran, A., Odagaki, H., and Hayase, M., 1997, "Dynamics and control of underactuated brachiation robots," In Proceedings of IEEE/ASME International Conference on Advanced Intelligent Mechatronics, pp. 98–.

[11] Lee, K., 1998, *Swing-up and balancing control of underactuated robotic systems* University of Illinois at Urbana-Champaign.

[12] Birglen, L., Laliberté, T., and Gosselin, C. M., 2007, *Underactuated robotic hands*, Vol. 40 Springer.

[13] Laliberte, T., Birglen, L., and Gosselin, C., 2002, "Underactuation in robotic grasping hands," *Machine Intelligence & Robotic Control,* **4**(3), pp. 1–11.

[14] Fattah, A., and Agrawal, S. K., 2004, "On the Design of Cable-Suspended Planar Parallel Robots," *Journal of Mechanical Design,* **127**(5), 10, pp. 1021–1028.

[15] Mustafa, S. K., Yang, G., Yeo, S. H., and Lin, W., 2008, "Kinematic calibration of a 7-dof self-calibrated modular cable-driven robotic arm," In 2008 IEEE International Conference on Robotics and Automation, pp. 1288–1293.

[16] Birglen, L., and Gosselin, C., 2003, "On the force capability of underactuated fingers," In 2003 IEEE International Conference on Robotics and Automation (Cat. No.03CH37422), Vol. 1, pp. 1139–1145 vol.1.

[17] Birglen, L., and Gosselin, C., 2004, "Kinetostatic analysis of underactuated fingers," *IEEE Transactions on Robotics and Automation,* **20**(2), pp. 211–221.

[18] Birglen, L., and Gosselin, C. M., 2006, "Optimally unstable underactuated gripper: Synthesis and applications," In 30th Annual Mechanisms and Robotics Conference, Parts A and B, Vol. 2, pp. 3–11.

[19] Birglen, L., and Gosselin, C. M., 2005, "Geometric Design of Three-Phalanx Underactuated Fingers," *Journal of Mechanical Design,* **128**(2), 04, pp. 356–364.

[20] Birglen, L., and Gosselin, C. M., 2006, "Force analysis of connected differential mechanisms: Application to grasping," *The International Journal of Robotics Research,* **25**(10), pp. 1033–1046.

[21] Odhner, L. U., Jentoft, L. P., Claffee, M. R., Corson, N., Tenzer, Y., Ma, R. R., Buehler, M., Kohout, R., Howe, R. D., and Dollar, A. M., 2014, "A compliant, underactuated hand for robust manipulation," *The International Journal of Robotics Research,* **33**(5), pp. 736–752.

[22] Schempf, H., 1990, "Comparative design, modeling, and control analysis of robotic transmissions," PhD thesis, Massachusetts Institute of Technology.

[23] Kevac, L. B., and Filipovic, M. M., 2022, "Development of cable-suspended parallel robot, cpr system, and its sub-systems," *Zbornik Radova*, pp. 318–354 vol.1.

[24] Étienne, L., Cardou, P., Métillon, M., and Caro, S., 2022, "Design of a planar cable-driven parallel crane without parasitic tilt," *Journal of Mechanisms and Robotics,* **14**(4).

[25] Liu, H., Gosselin, C., and Laliberté, T., 2012, "Conceptual design and static analysis of novel planar spring-loaded cable-loop-driven parallel mechanisms," *Journal Mechanisms Robotics*.

[26] Khakpour, H., and Birglen, L., 2014, "Workspace augmentation of spatial 3-dof cable parallel robots using differential actuation," In 2014 IEEE/RSJ International Conference on Intelligent Robots and Systems, IEEE, pp. 3880–3885.

[27] Khakpour, H., Birglen, L., and Tahan, S.-A., 2014, "Synthesis of differentially driven planar cable parallel manipulators," *IEEE Transactions on Robotics,* **30**(3), pp. 619–630.

[28] Behroozi, F., Cardou, P., and Caro, S., 2023, "Transmission systems to extend the workspace of planar cable-driven parallel robots," In Cable-Driven Parallel Robots, S. Caro, A. Pott, and T. Bruckmann, eds., Springer Nature Switzerland, pp. 308–320.

[29] Gouttefarde, M., and Gosselin, C. M., 2004, "On the properties and the determination of the wrench-closure workspace of planar parallel cable-driven mechanisms," In International Design Engineering Technical Conferences and Computers and Information in Engineering Conference, Vol. 46954, pp. 337–346.

[30] Gouttefarde, M., and Gosselin, C. M., 2006, "Analysis of the wrench-closure workspace of planar parallel cable-driven mechanisms," *IEEE Transactions on Robotics,* **22**(3), pp. 434–445.

[31] Roberts, R. G., Graham, T., and Lippitt, T., 1998, "On the inverse kinematics, statics, and fault tolerance of cable-suspended robots," *Journal of Robotic Systems,* **15**(10), pp. 581–597.

[32] Meyer, C. D., 2001, *Solutions manual: Matrix analysis and applied linear algebra* SIAM: Society for Industrial and Applied Mathematics.

[33] Gouttefarde, M., Merlet, J.-P., and Daney, D., 2007, "Wrench-feasible workspace of parallel cable-driven mechanisms," In Proceedings 2007 IEEE International Conference on Robotics and Automation, pp. 1492–1497.